Pulse Density Modulation Based Mutual Inductance and Load Resistance Identification Method for Wireless Power Transfer System

Ruimin Dai, Wei Zhou, *Member, IEEE*, Yonghong Chen, Zhehui Zhu, and Ruikun Mai

***Abstract*—In wireless power transfer (WPT) system, the information of mutual inductance and load resistance is usually needed for the front-end to regulate power and efficiency. To acquire the values of these two parameters without wireless communication system and without affecting the output power, this article proposes an identification method based on the pulse density modulation (PDM) technique. The underlying principle is to obtain a range of interharmonics by altering the sequence of PDM. First, the PDM strategy brings in interharmonics, which can be identified through fast Fourier transmission (FFT). Then, these interharmonics are used to established multiple sets of equation related to front-end impedance and the two unknowns. Finally, with the least-square approximation, mutual inductance and load resistance can be estimated. This article notices that the sequence of PDM strategy could affect the amplitudes of interharmonics, and selects the sequences to maximize the magnitudes for less sensitivity to measurement errors. Experimental results show that the relative errors of identification are less than 5% when the nominal values of capacitors are the same as actual values, and reach 7.40% when considering the nominal values may deviate from the actual values. Besides, the output power and efficiency are not affected during the identification process. This proposal requires only magnitudes of voltage and current in the transmitter side, no other hardware is needed, and works with the fixed frequency, which is suitable for any frequency range.**

***Index Terms*—Inductive power transfer (IPT), load estimation, mutual inductance estimation, pulse density modulation (PDM).**

I. Introduction

COMPARED with traditional plugin charging, wireless power transfer (WPT) system has the advantages of being safe, convenient, and flexible [1], [2]. Because of these merits, WPT technology is a promising charging method for electrical vehicles, implantable biomedical devices, and some other special situations where direct charging is impossible [3]–[5]. Generally, a WPT system needs to provide the required power to the load and work with the highest possible efficiency [6]. Traditionally, a communication system that sends signal between transmitter (also called front-end) and receiver is used to regulate power and improve efficiency. For instance, study in [7] uses wireless communication to regulate the output power, and the proposal in [8] applies wireless communication to find the optimum efficiency point. However, a wireless communication system increases the size, cost, and complexity of the overall system. Therefore, many research works have been explored to improve the performance of WPT system without wireless communication. Methods to identify the mutual inductance and load resistance without the communication system have been intensively studied [9]. These identification methods can be roughly divided into four categories.

1) Nonzero receiver reactance method.
2) Energy injection method.
3) Reconfigurable circuit method.
4) Frequency sweeping method.

The following paragraph will briefly discuss these categories.

1) Nonzero receiver reactance method was firstly used by Madawala [10]. Based on LCL-P (series-parallel-series-compensated transmitter and parallel-compensated receiver) topology, through obtaining the real and imaginary components of voltage on transmitter capacitor, the values of mutual inductance and voltage on load can be acquired. This method has the advantages of simple calculation and fast monitoring, and is implemented for controlling the output voltage of inductive power transfer (IPT) system [10], [11]. The limitation is that this method is only suitable for systems that have the nonzero receiver reactance when the working frequency equals the receiver resonant frequency.
2) Energy injection method was first proposed by Wang to detect the load [12]. This way involves two modes of operation: energy injection mode and free oscillating mode. Decay rate of transmitter current in the free oscillating period depends on the mutual inductance and load. Study in [13] proves that the load is inversely proportional to the current decay rate. One problem of the above studies is that only the load is detected while mutual inductance is assumed to be known. Another limitation is that the

Manuscript received April 21, 2021; revised November 2, 2021; accepted February 15, 2022. Date of publication February 23, 2022; date of current version April 28, 2022. This work was supported in part by the National Natural Science Foundation of China under Grant 51907170, in part by the Sichuan Science and Technology Program under Grant 2021YFH0039, and in part by the Sichuan Youth Science and Technology Innovation Research Team under Grant 2020JDT0004. Recommended for publication by Associate Editor O. C. Onar. *(Corresponding author: Wei Zhou.)*

The authors are with the Southwest Jiaotong University, Sichuan 611756, China (e-mail: ruimindai1992@163.com; wzhou@swjtu.edu.cn; 723856431@qq.com; 285089064@qq.com; mairk@swjtu.cn).

Color versions of one or more figures in this article are available at https://doi.org/10.1109/TPEL.2022.3153657.

Digital Object Identifier 10.1109/TPEL.2022.3153657

output power is discrete, thus, this method is only useful in applications where just the initial value of the load is needed.

3) Reconfigurable circuit method. This way involves changing the topology. Su proposed an identification method involving switching capacitors to convert the system between two different circuits [14]. Through analyzing transmitter current and resonant frequency in these two circuits, mutual inductance and load resistance can be calculated. The drawback is that switches inevitably increase the overall size. Study in [15] proposes that when the receiver is shorted, through evaluating the phase difference between the switching signal of the inverter and the transmitter current, mutual inductance can be calculated. The limitation of this study is that load identification is not considered, and the power deliver is paused during identification.
4) Frequency sweeping method. The principle of this way is that the impedance of the transmitter side is affected by frequency and other circuit quantities. Thus, if all the rest parameters are given, by collecting impedance at a range of different frequency points, the unknown parameters can be determined by solving the mathematical equations. Yin proposed that by measuring the amplitudes and phase shift of the input voltage and current at a designed frequency, the mutual inductance and load resistance can be calculated [16]. Except for mutual inductance and load, the frequency sweeping method can also be used to estimate other circuit parameters [17]. Yang applied this method in a two-receiver IPT system and proves that capacitor, inductor, mutual inductance, and load resistance can be identified [18]. For these studies, one problem is that output power is not maintained. This is because the power depends on load and frequency, and load is required to be constant during the identification. Consequently, if there is no other adjustment, the power at each frequency point will be different. Another limitation is that working at a nonresonant frequency will increase switching losses and reactive power, resulting to an efficiency decline.

Besides, some other researches on maintaining the output power during identification are also worth mentioning. Study in [19] puts forward two inverters on transmitter side to keep the output. The problem is that adding extra inverter inevitable costs size. Proposal in [20] uses fundamental and third-order harmonics to identify parameters, the limitation is that the third-order harmonic signal may be very small, making it sensitive to measurement error. Besides, this study adopts only two frequency points for estimation, while it is pointed out in [21] that due to measurement error and parameter tolerance, only two frequency points may not be enough to obtain a very accurate solution.

This article proposes a method that uses pulse density modulation (PDM) strategy to estimate mutual inductance and load resistance for inductively power transfer (IPT) system. The background of PDM technology is briefly introduced as follows: PDM technology was first mentioned in [22] and then proved by H. Fujita as an efficient control method for power converter because its zero-voltage-switching (ZVS) can be maintained during power regulation [23]. Then, Calleja found that frequency spectrum of PDM waveform contains a range of interharmonics [24], where interharmonics are defined as frequencies that are not integer multiples of the fundamental frequency [25]. PDM technique was then introduced to IPT system. Li proposed PDM-based full-bridge converter for IPT system, which was proved to achieve both voltage regulation and efficiency maximization without dc/dc converters [26].

TABLE I
FEATURES OF THE IDENTIFICATION METHODS

Method \ Feature	Online	No extra hardware	Output maintained	Working frequency
Non-zero receiver reactance [10, 11]	✓	✓	✓	Fixed at receiver resonant frequency
Energy injection [12, 13]	×	✓	×	
Reconfigurable Circuit [14, 15]	✓	×	×	Fixed and full frequency range
Frequency Sweeping [16-18]	✓	✓	×	Frequency sweeping required
Dual-Inverter [19]	✓	×	✓	Fixed and Full frequency range
Proposed	✓	✓	✓	

The motivations and contributions of this article are concluded as follows:

1) Output power and efficiency can be maintained during the identification process.
2) No extra hardware, only voltage and current magnitudes on the transmitter are needed for estimation.
3) Working frequency is fixed to reduce the control complexity and is suitable for any frequency range.
4) Reduce the sensitivity to measurement errors by selecting the maximum magnitude of interharmonics.

The features of previous papers and this paper are listed in Table I, where "online" means that the identification can be performed again if required.

This article is organized as follows: Section II analyzes the theory. The Section III designs an experimental prototype for verification. The final section discusses the conclusions and future work.

II. Theoretical Analysis

A. Characteristics of SS Topology

series-series compensated (SS) topology is one of the most widely used IPT circuits [27], [28]. A typical SS-based IPT system is shown in Fig. 1, the subscripts "1" and "2" are used to denote the transmitter-side and receiver-side parameters, respectively. L (C) represents the inductor (capacitor). E (I_{di}) is the dc input voltage (current). M is the mutual inductance, R_L is dc load. R_1 (R_2) is the equivalent series resistance (ESR) of transmitter (receiver) coil. U_{do} (I_{do}) represents the voltage (current) on dc load. The inverter is composed of four MOSFETs (Q1–Q4), the rectifier is constituted by four diodes (D1–D4).

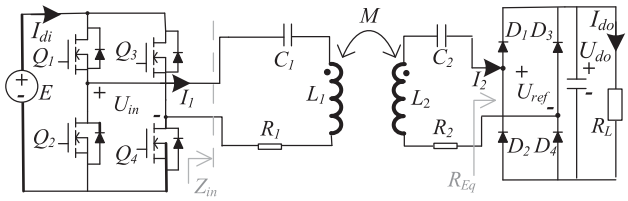

Fig. 1. SS-based IPT system.

In this article, the combination of the rectifier and R_L is viewed as an equivalent resistor: R_{Eq}, where $\mathrm{R_{Eq}} = (8/\pi^2)\mathrm{R_L}$. The angular frequency is represented by ω, where $\omega = 2\pi f$, f is operating frequency. The coils are designed to operate with resonant frequency: f_0. Since $\omega_0 = 2\pi f_0$, equations can be derived as follows:

$$\omega_0^2 L_i C_i = 1, \text{where } i = 1, 2. \tag{1}$$

Based on Kirchhoff's Voltage Law, the SS topology shown in Fig. 1 can be described as (2), where $\dot{U}_{\mathrm{in}}$ is the input voltage vector, which is referenced as zero phase degree. $\dot{I}_1(\dot{I}_2)$ is the transmitter (receiver) current vector. The input impedance Z_{in} shown in Fig. 1 is defined as $Z_{\mathrm{in}} = \dot{U}_{\mathrm{in}}/\dot{I}_1$. By solving (2), Z_{in} can be represented in (3)

$$\begin{cases} \dot{U}_{in} = \left[R_1 + j\left(\omega L_1 - \frac{1}{\omega C_1}\right)\right]\dot{I}_1 + j\omega M\dot{I}_2 \\ 0 = j\omega M\dot{I}_1 + \left[R_2 + R_{Eq} + j\left(\omega L_2 - \frac{1}{\omega C_2}\right)\right]\dot{I}_2 \end{cases} \tag{2}$$

$$Z_{in} = R_1 + j\left(\omega L_1 - \frac{1}{\omega C_1}\right) + \frac{(\omega M)^2}{R_2 + R_{Eq} + j(\omega L_2 - \frac{1}{\omega C_2})}. \tag{3}$$

Based on (3), if ω changes to another value, a new set of $\{\omega, Z_{in}\}$ can be obtained. One set of $\{\omega, Z_{in}\}$ corresponds to one equation of (3). Assuming that values of R_1, R_2, L_1, L_2, C_1, and C_2 are given, then, the unknowns $\{M, R_{Eq}\}$ can be calculated from two equations of (3). This is the basic principle for designing parameter identifying. In addition to SS topology, this principle is also applicable to other topologies, just by modifying the equation in (3) to the Z_{in} equation of the relevant topology.

From the front-end, the magnitude of Z_{in} can be easily obtained by measuring the magnitudes of voltage and current as shown in (4), where $|Z_{in\_\omega}|$ denotes the amplitude of Z_{in} at frequency ω, $|U_{in\_\omega}|$ ($|I_{1\_\omega}|$) is the amplitude of the $\dot{U}_{\mathrm{in}}$ ($\dot{I}_1$) at frequency ω

$$|Z_{in\_\omega}| = |U_{in\_\omega}|/|I_{1\_\omega}|. \tag{4}$$

Therefore, the process for identifying M and R_{Eq} can be derived as follows: First, obtaining at least two sets of $\{\omega, |Z_{in\_\omega}|\}$ from the front-end based on (4). Then, according to the relationship between $|Z_{in\_\omega}|$ and $\{M, R_{Eq}\}$, the two unknowns can be derived by solving at least two equations of (3).

B. Least-Square Approximation

It is important to notice that, for a mathematical equation which is error-free, M and R_{Eq} solved by any two equations of (3) will be identical. But in practical applications, because of the measurement errors and parameter tolerance, the sets $\{M, R_{Eq}\}$ derived from different equations of (3) will always be different. In order to find the most suitable $\{M, R_{Eq}\}$ for all the $\{\omega, |Z_{in\_\omega}|\}$ sets, the least-square approximation method is used.

The basic principle of the least-square problem is to find the minimum residuals. Group M and R_{Eq} into a vector of unknowns $X = (M, R_{Eq})^{\mathrm{T}}$, and the residuals r_j can be defined as (5). m is the number of equations. y_j is the value of $|Z_{in\_\omega}|$ at the jth set of $\{\omega, |Z_{in\_\omega}|\}$ sets, which are obtained from (4). Notation $|Z_{in}(j\omega, X)|$ is the amplitude of Z_{in} with frequency $j\omega$ and X, where $j\omega$ is the value of ω in the jth set of $\{\omega, |Z_{in\_\omega}|\}$ sets

$$r_j(X) = y_j - |Z_{in}(j\omega, X)|, j = 1, 2, \ldots m. \tag{5}$$

The estimated value X can be obtained by solving the problem in (6), where L (H) is the lower (upper) bound for X.

$$\min_{X\in[L,H]} f(X) = r_1^2(X) + r_2^2(X) + \cdots r_m^2(X). \tag{6}$$

Based on (3), M and R_{Eq} are nonlinearly related to $|Z_{in\_\omega}|$, thus, solving (6) is a nonlinear least-square problem. There are no direct equations for solving nonlinear least-square problem [29]. Thus, it is almost impossible to give explicit equations to show how the unknowns are calculated. According to previous studies [18], [20], [21], iteration calculation can be used in this situation for estimation. Many mathematical software (for instance, MATLAB, 1stopt [30]) can be used to do the iterations for solving (6).

C. PDM Technology

According to the analysis above, a crucial step for parameter identification is to create multiple sets of $\{\omega, |Z_{in\_\omega}|\}$. PDM technology is utilized to accomplish this task. Generally, it is preferred to meet these two demands during the identification process: First, the output power and efficiency are not affected by the identification process. Second, interharmonics with smaller magnitudes usually have relatively high sensitivity to measurement errors, so it is better to use interharmonics with larger amplitudes. This section will design the PDM strategy according to these two demands.

In PDM control scheme, working frequency keeps at f_0, so the resonant condition can be maintained. The operating principle of PDM can be represented as Fig. 2, where T_0 is the resonant period of the IPT system ($T_0 = 1/f_0$), $0.5T_0$ is half of the resonant cycle. The PDM technique works by connecting the circuit to the inverter during p half of the resonant cycle (denoted as "power mode"), and then short-circuiting the circuit during n half of the resonant cycle (denoted as "short mode"). The length of one PDM full cycle is $0.5(p+n)T_0$. The pulse density of PDM is defined as $p/(p+n)$.

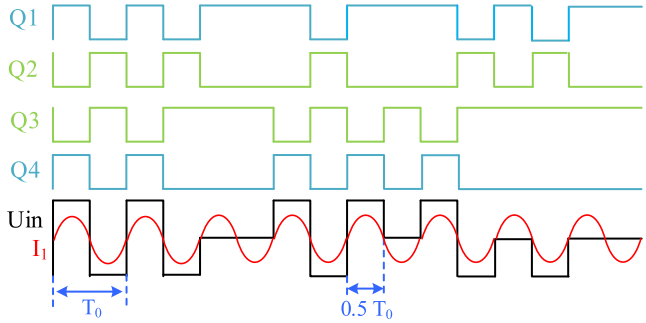

Fig. 2. PDM technique operating principle.

U_{in} can be represented as (7). With Fourier analysis, U_{f0M}, the amplitude at f_0 for output voltage, can be represented as (8)

$$U_{in} = \begin{cases} E & \text{in power mode if } I_1 \text{ is positive;} \\ -E & \text{in power mode if } I_1 \text{ is negative;} \\ 0 & \text{in short mode} \end{cases} \tag{7}$$

$$U_{f0M} = \frac{4E}{\pi}\frac{p}{p+n} = \frac{4E}{\pi}\text{density}. \tag{8}$$

Based on (8), U_{f0M} is proportional to pulse density [denoted as "density" in (8)]. In order to keep the power constant, pulse density should be fixed during the identification. Study in [31] mentions that to reduce the ripple of output voltage, the PDM sequences should be distributed as evenly as possible. For simplicity, density is set to 0.5 in this article, which means the system has the same power-mode time and short-mode time, which helps evenly distributing. Notice that the values of density, p, and n does not affect the process of selecting frequency points and sequences.

The interharmonics brought by PDM will be used to create multiple frequency points. Compared with the traditional frequency sweeping method, using PDM interharmonic has the advantages of maintaining the resonant working condition and not affecting the output power, but the locations of frequency points in interharmonics are constrained by (9) (given 0.5 density). The smallest value of p is 2. And the interharmonics equal to or larger than $2f_0$ are ignored because their magnitudes are usually relatively small and require higher sampling rate

$$f_j = \left(1 \pm \frac{j}{p}\right) f_0, j = 1, 2, \ldots p-1. \tag{9}$$

Based on (9), if $p = 2$, there are 2 interharmonics as: $f_0/2$ and $3f_0/2$; if $p = 3$, there are 4 interharmonics as: $f_0/3$, $2f_0/3$, $4f_0/3$, and $5f_0/3$; if $p = 4$, there are 6 interharmonics as: $f_0/4$, $2f_0/4$, $3f_0/4$, $5f_0/4$, $6f_0/4$, and $7f_0/4$; if $p = 5$, there are 8 interharmonics as $f_0/5, 2f_0/5, 3f_0/5, 4f_0/5, 6f_0/5, 7f_0/5, 8f_0/5$, and $9f_0/5$. Thus, by sweeping p from 2 to 5, the system could obtain 20 points. Notice that these points will be filtered further because some points are repeated, for example, point $f_0/2$ of $p = 2$ is the same location as the point $2f_0/4$ of $p = 4$. Besides, some points are likely to be interfered by adjacent points, and some points may be too small to be detected by the sensor circuits, these problems will be discussed later.

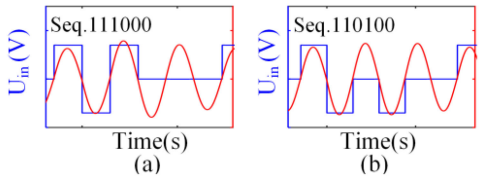

Fig. 3. Different sequences for $p = 3$ (a). Seq. 111000 (b). Seq. 110100.

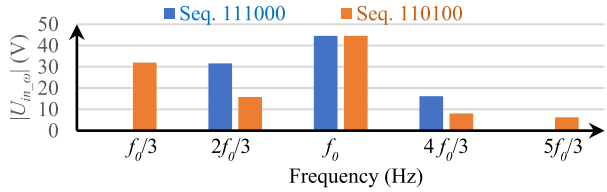

Fig. 4. Frequency spectrum for $p = 3$, where $E = 70$ V.

Since it is necessary to create multiple points, and at each point the sequence with maximum magnitude is preferred for data collection, the process for sequences selecting can be derived as follows: first, for each p, designing more than one waveform if possible. To distinguish the waveforms, they are named as Seq. x, where each x represents the mode in $0.5T_0$: if x equals 1/0, the system is in power/short mode; the number of x equals $p+n$. The key function of multiple waveforms is that with the same p, the waveforms will have the same set of frequency locations, but they are likely to have different magnitudes for each location. Then, with fast Fourier transmission (FFT), the frequency spectrums can be derived to analyze the magnitudes of interharmonics. Finally, at each frequency point, the sequence with the maximum magnitude will be adopted.

To help understand, taking $p = 3$ as an example. At least two sequences can be created as illustrated in Fig. 3. Next, with the help of FFT method, the frequency spectrums can be illustrated as Fig. 4, it can be concluded that the two sequences have the same U_{f0M} as $2E/\pi = 44.6$ according to (8).

Based on Fig. 4, for sequence 111000, $|U_{in\_\omega}|$ for $f_0/3$ and $5f_0/3$ are zero, while the amplitudes for $2f_0/3$, $4f_0/3$ are larger than that for sequence 110100. Therefore, for $p = 3$, amplitudes of $|U_{in\_\omega}|$ and $|I_{1\_\omega}|$ at $f_0/3$, $5f_0/3$ ($2f_0/3$, $4f_0/3$) are collected when sequence is 110100 (111000).

For $p = 2$, only one sequence exists: 1100, thus, this sequence will be directly adopted. For $p = 4, 5$, at least five sequences exist as illustrated in Figs. 5 and 6, respectively, the spectrums for $p = 2$, 4, and 5 can be derived as Figs. 7–9.

Based on Figs. 7–9, it can be concluded that only the maximum magnitude is not sufficient for selecting, for instance, both Seq. 1011110000 (orange) and Seq. 1010101100 (gold) at $f_0/5$ in Fig. 9 have the maximum magnitudes. And as mentioned before, some locations are repeated. To help selecting points and sequences, interference from adjacent is considered [32], notice that the unused points and sequences does not necessarily mean poor estimation result, it is just better to not use them for spectrum analysis.

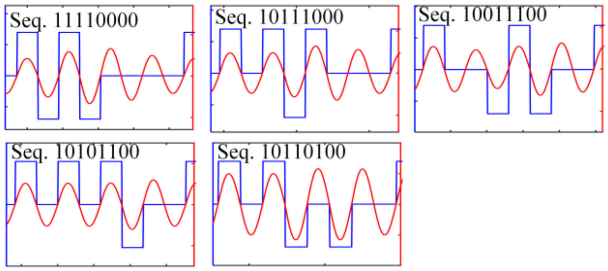

Fig. 5. Different sequences for $p = 4$, where blue (red) wave is U_{in} (I_1).

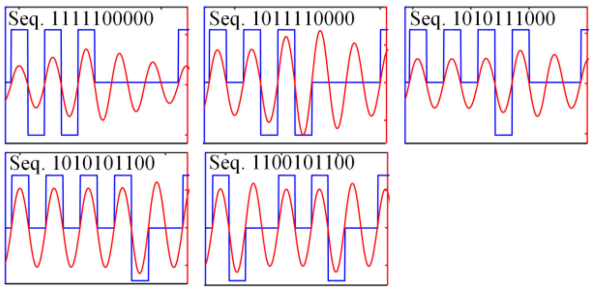

Fig. 6. Different sequences for $p = 5$, where blue (red) wave is U_{in} (I_1).

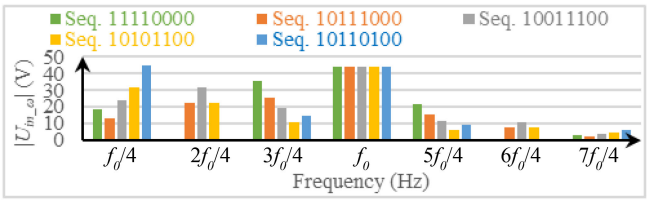

Fig. 8. Frequency spectrum for $p = 4$, where $E = 70$ V.

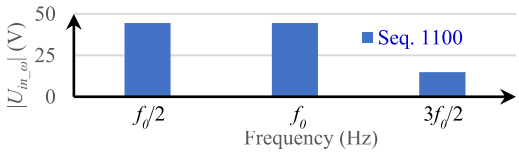

Fig. 7. Frequency spectrum for $p = 2$, where $E = 70$ V.

For selecting, two criteria are adopted as follows: the first criterion is to start collecting from small p value. Because based on (9), smaller p involves less interharmonics. The smaller the number of interharmonics, the larger the gap between interharmonics, and the less the interference to spectrum analysis. Thus, $f_0/2$ and $3f_0/2$ in Fig. 7 will be used while $2f_0/4$ and $6f_0/4$ in Fig. 8 will not be used. The second criterion is that, based on [32], the larger/smaller the adjacent interharmonics, the more/less the interference for identifying the other interharmonics. Therefore, if the gap between f_0 (this point has the maximum magnitude) and its two adjacent points is too small, these adjacent points are likely to be interfered. That means points $3f_0/4$ and $5f_0/4$ in Fig. 8, and $4f_0/5$ and $6f_0/5$ in Fig. 9 are better not to be used. Furthermore, this second criterion plays an important guiding role in selecting sequences when more than one sequences have

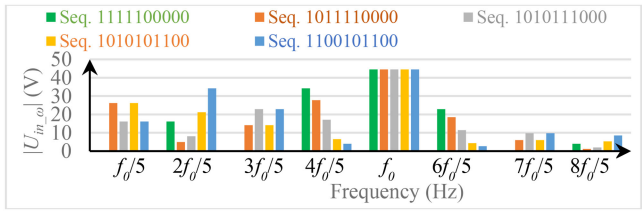

Fig. 9. Frequency spectrum for $p = 5$, where $E = 70$ V.

TABLE II
PROPER SEQUENCES

Seq No.	Sequence	Frequency Point
1	1100	f_0, $f_0/2$, $3f_0/2$
2	110100	$f_0/3$, $5f_0/3$
3	111000	$2f_0/3$, $4f_0/3$
4	10110100	$f_0/4$, $7f_0/4$
5	1011110000	$f_0/5$
6	1100101100	$2f_0/5$, $3f_0/5$, $7f_0/5$, $8f_0/5$

the maximum magnitudes: the sequence with smaller magnitude in the adjacent point is preferred. That means for $f_0/5$ in Fig. 9, Seq. 1011110000 (orange) is selected rather than Seq. 1010101100 (gold) because the former one has smaller magnitude in $2f_0/5$. Another tricky thing is that, for $3f_0/5$ in Fig. 9, Seq. 1100101100 (blue) is larger than 1010111000 (grey) at one adjacent point $2f_0/5$, but the situation is reversed at another adjacent point $4f_0/5$. To solve this problem, control strategy is taken into consideration. The lesser the variation, the simpler the control strategy. Since Seq. 1100101100 (blue) has the maximum magnitudes for $2f_0/5$, $7f_0/5$, and $8f_0/5$, this sequence will also be used for $3f_0/5$. Finally, for the rest points: $f_0/4$ and $7f_0/4$ in Fig. 8, Seq. 10110100 (blue) will be used for the maximum magnitudes.

Consequently, the proper sequences for maximizing interharmonics can be concluded in Table II. These sequences will be used in this paper for collecting $|U_{in\_\omega}|$ and $|I_{1\_\omega}|$.

Based on Table II, by sweeping the sequence from Seq 1 to Seq 6, there are 14 frequency points. The number of frequency points for reasonably accurate estimations depends on the practical system configuration. For instance, 2 points are used in [20] for estimating two unknowns, 20 points are used in [21] for identifying two unknowns, and 38 points are used in [18] for determining nine unknowns. Besides, due to the system parameters, at some point, $|I_{1\_\omega}|$ may be too small to be measured, causing that point unusable. And since M and R_{Eq} are not given, it is almost impossible to predetermine which point will have small $|I_{2\_\omega}|$. In addition, whether a point is appropriate also depends on actual setup, the high-quality sensors can accurately obtain the small signals and high-frequency signals that cannot be acquired by the poor sensors. These problems can be described as that the usable points in Table II cannot derive a good estimation result, one of the methods to solve it is to increase the value of p to bring in more interharmonics, and using the new points together with the usable points in Table II for parameter identification.

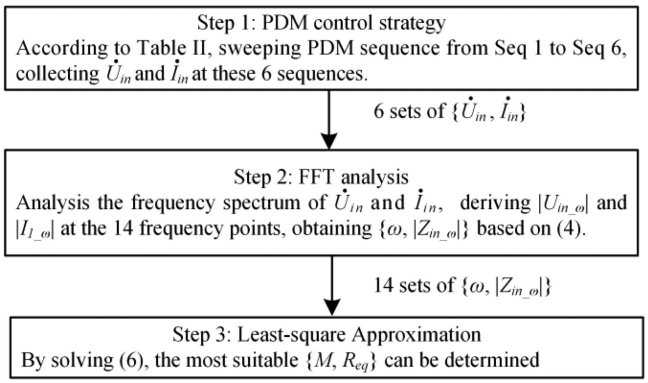

Fig. 10. Process for parameter identification in this article.

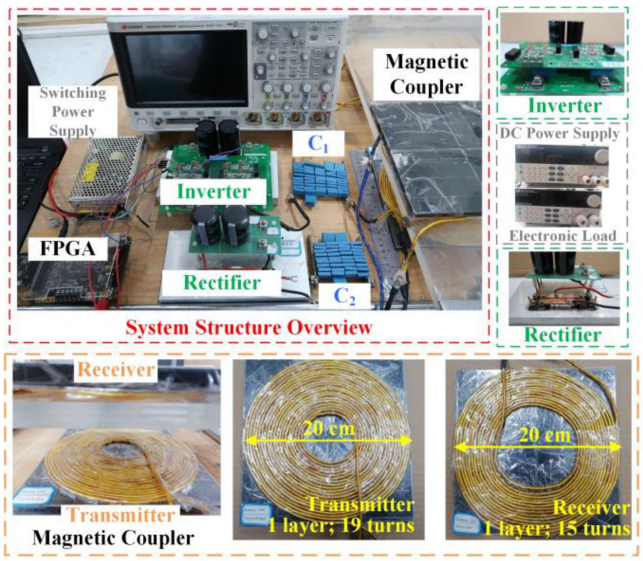

Fig. 11. Experimental prototype.

D. Conclusion of the Proposed Method

The process for the parameter identification method can be concluded in Fig. 10.

III. Experimental Verification

As shown in Fig. 11, an experimental prototype of SS-compensated IPT system is built. This experimental setup is only used to demonstrate the feasibility of the theoretical analysis. For different applications in real practice, the size and power capacity can be scaled down/up accordingly.

A. Experimental Setup

The full-bridge inverter is composed of four MOSFETs (CREE C2M0080120D). The switching signal of MOSFETs is provided by an FPGA (ALINX AX7020). The switching power supply is used to power the driver board of inverter. The rectifier is constituted by 4 diodes (DESI 2x 61-04C). The inductors are wound with Litz wire (0.1∗400, 2.85 mm width). The receiver pad is centered on top of transmitter pad, ferrite (1 cm thickness) is inserted for enhancing and guiding the flux, and it is assumed that the ferrite does not saturate under normal operation. LCR meter (Agilent E4980A) is applied to measure the values of inductance, capacitance, and ESR. The waveforms are analyzed and recorded by the oscilloscope (Keysight infiniiVision DSOX3014T). The dc power supply (ITECH IT6942A 60V/15A/360W) and electronic load (ITECH IT8812C 120V/60A/250W) are applied as E and R_L to run the system, respectively.

TABLE III
Cases for Identification

Case	M (uH)	R_L (R_{EQ}) (Ω)	Gap (cm)	L1 (uH)	L2 (uH)	C1 (nF)	C2 (nF)	R_1 / R_2 (Ω)
1	14.50	12 (9.73)	9.5	85.71	69.72	40.94	50.61	0.2
2		15 (12.16)						
3	20.47	22 (17.83)	8.0	87.20	70.61	40.37	49.89	0.2
4		25 (20.26)						

TABLE IV
Parameters for Least-Square Approximation

Parameter	Lower bound	Upper bound	Parameter	Lower bound	Upper bound
M	5uH	30uH	R_{Eq}	1Ω	30Ω

TABLE V
Sample Rate for Data Collection

Seq Number	1	2	3	4	5	6
Maximum Signal Frequency (kHz)	127.50	141.67	141.67	148.75	136	136
Sample Frequency (MHz)	1.28	1.42	1.42	1.49	1.36	1.36

B. Parameter Identification

Four cases for identification are designed as shown in Table III, where gap is the vertical distance between transmitter and receiver. f_0 is set as 85 kHz just for theoretical verification. The parameters for the least-square approximation are shown in Table IV, these values are determined according to practice and experience.

Based on Nyquist criterion, the sample rate must be at least twice the maximum signal frequency. This article sets the sample rate to 10 times the maximum signal frequency. Thus, based on Table II, the sample frequencies can be designed as Table V.

To achieve the sample rate in Table V, many hardware setups can be used, for instance, the combination of current sensor MCX 1101 (1.5 MHz bandwidth) and analog-to-digital converter AD7760 (2.5 MSPS sampling rate, 24 bit). The proposed identification method is applicable to any resonant frequency. For different applications in real practice, the hardware setups can be modified accordingly. This experiment is only used to demonstrate the feasibility of the theory, thus, for simplicity, the data is collected through oscilloscope, and then being extracted to computer and MATLAB is used for analyzing.

For the four cases, Fig. 12 shows the identification results, where the dotted line represents the nominal value, the values of horizontal axis are explained in Table VI. The initial value for

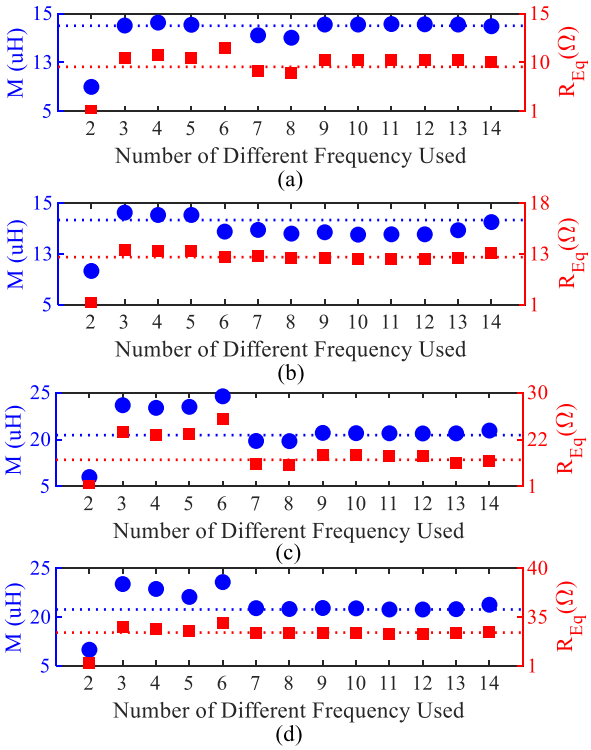

Fig. 12. Identified M (blue dot) and R_{Eq} (red square). The dotted line represents the nominal value. (a). Case 1 (b). Case 2 (c). Case 3 (d) Case 4.

TABLE VI
CORRESPONDING FREQUENCY POINTS FOR ESTIMATION

Number of Frequency used	Corresponding Frequency Point
2	$f_0/2$, f_0
3	Points above + $3f_0/2$
4	Points above + $f_0/3$
5	Points above + $2f_0/3$
6	Points above + $4f_0/3$
7	Points above + $5f_0/3$
8	Points above + $f_0/4$
9	Points above + $7f_0/4$
10	Points above + $f_0/5$
11	Points above + $2f_0/5$
12	Points above + $3f_0/5$
13	Points above + $7f_0/5$
14	Points above + $8f_0/5$

number of frequencies used is 2 because there are two unknowns to be identified. The frequency used for estimation starts from small p. As multiple interharmonics may share the same p, the smaller frequency point is used first for identification due to it requires less sampling rate.

Based on Fig. 12 when only two frequency points are applied to identify the unknowns, the results are poor, this phenomenon shows the existence of measurement errors and parameter tolerance. The measurement error is unpredictable and the number of frequency points required to obtain an acceptable result depends on the practical setup. In this experiment, a reasonably accurate estimation can be acquired from around seven different frequency points. After the 7th point, the estimated value fluctuates around the reference value within 5%. The estimation results

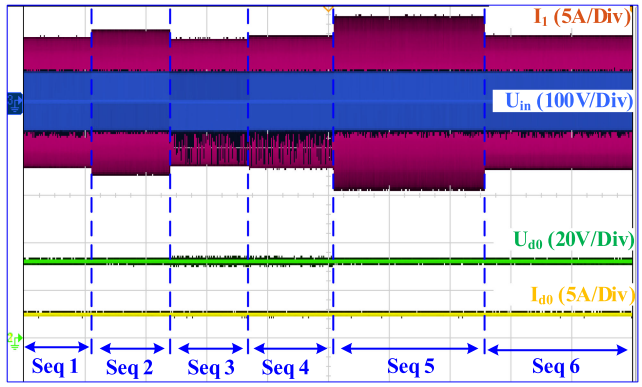

Fig. 13. Captured waveforms of voltages and currents output from inverter (U_{in}, I_1) and on dc load (U_{do}, I_{do}) for Case 1 as sequence changes, where $E = 60$ V.

(relative error) at the 7th point for the four cases are as follows: Case 1: $M = 14.01$ uH (3.38%), $R_{Eq} = 9.35\ \Omega$ (3.91%); Case 2: $M = 14.10$ uH (2.76%), $R_{Eq} = 12.02\ \Omega$ (1.15%); Case 3: $M = 19.83$ uH (3.13%), $R_{Eq} = 16.97\ \Omega$ (4.82%); Case 4: $M = 20.06$ uH (2.00%), $R_{Eq} = 20.50\ \Omega$ (1.19%). As the number of frequencies used increases, the estimated results have some fluctuations. This appearance is caused by the measurement error and is very common that can also be observed in [21, Fig. 7]. Although the fluctuation exists, the least-square method enables the estimated results to converge towards the reference value as the number of frequency points increases.

The computer used to do the iteration task in this study is ThinkPad T450S (Intel Core i5-5200U @2.2 GHz, 8 GB RAM), it takes from 2 to 5 s to obtain the estimated M and R_{Eq} for one case. This consumed time makes this proposal unsuitable for situations requiring fast monitoring, but compared with several hours of battery charging time, this time is ignorable. Thus, this proposal is more suitable for stationary charging, e.g., stationary electrical vehicle charging system.

C. Voltage and Current During Sequence Sweeping

As mentioned before, the system outputs are important features. Fig. 13 represents the voltages and currents for Case 1. The U_{do} and I_{do} are fixed as the sequence changes, proving that the proposal can achieve constant outputs during the identifying process.

The sequence has influence on I_1. Based on Fig. 13, Seq 1, Seq 3, and Seq 6 have the minimum peak value of I_1, while Seq 5 has the maximum peak value of I_1. The fluctuation of I_1 is caused by the number of rising and falling processes, which is analyzed in [33]. The U_{in} and I_1 waveforms for Seq 1 and Seq 5 are shown in Fig. 14. I_1 slightly lags behind U_{in}, which helps to achieve the ZVS condition.

D. Transferred Efficiency and Power

The IPT system is usually required to provide power stably. The efficiency and power characteristics for Case 1 are represented in Fig. 15. From Seq 1 to Seq 6, the variations are

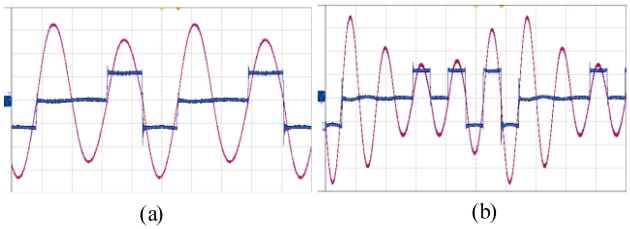

Fig. 14. Captured waveforms [5 μs/Div for (a) and 10 μs/Div for (b)] for U_{in} (blue, 50 V/Div), I_1 [red, 2 A/Div for (a) and 2.5 A/Div for (b)] for Case 1, where $E = 60$ V. (a). Seq 1 (1100) (b). Seq 5 (1011110000).

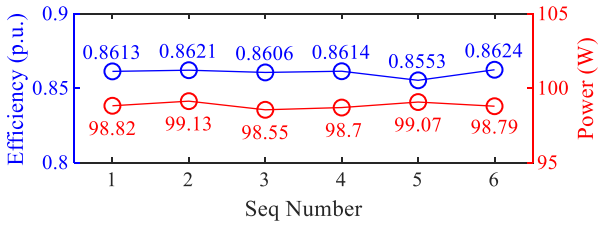

Fig. 15. Efficiency (blue) and power (red) for Case 1, where $E = 60$.

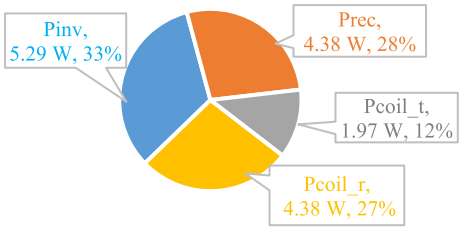

Fig. 16. Power loss breakdown for Seq 1 in Case 1, where Pinv (Prec) represents power loss in inverter (rectifier), Pcoil_t (Pcoil_r) represents power loss in transmitter (receiver) resonant tank.

less than 1% for both efficiency and power, proving that the proposed identification method can afford constant power. The power loss distribution for Seq 1 in Case 1 is illustrated in Fig. 16. Power losses are determined based on [34], [35], and practical measurements.

E. Influence of Measurement Errors

In the experiment, the magnitudes of $\dot{U}_{\text{in}}$ and $\dot{I}_1$ are used to calculate $|Z_{in\_\omega}|$. Equivalently, the measured parameters can be regarded as one variable: $|Z_{in\_\omega}|$. The relationship between $|Z_{in\_\omega}|$ and M and R_{Eq} can be represented by (10), where φ denotes the angular between $\dot{U}_{\text{in}}$ and $\dot{I}_1$. Based on (10), by taking the derivative of $M\,(R_{Eq})$ to $|Z_{in\_\omega}|$, the rate of change of $M\,(R_{Eq})$ with respect to measurement error can be represented as Fig. 17

$$\begin{cases} A = |Z_{in\_\omega}|\cos(\varphi) - R_1 B = |Z_{in\_\omega}|\sin(\varphi) - \omega L_1 + \frac{1}{\omega C_1} = \\ M = \sqrt{\frac{(\omega L_2 - \frac{1}{\omega C_2})(A^2+B^2)}{-\omega^2 B}} R_{Eq} = -\frac{(\omega L_2 - \frac{1}{\omega C_2})A}{B} - R_2 \end{cases}. \tag{10}$$

Fig. 17 shows that at the resonant point, the sensitivity to measurement error is high. Notice that this does not necessarily

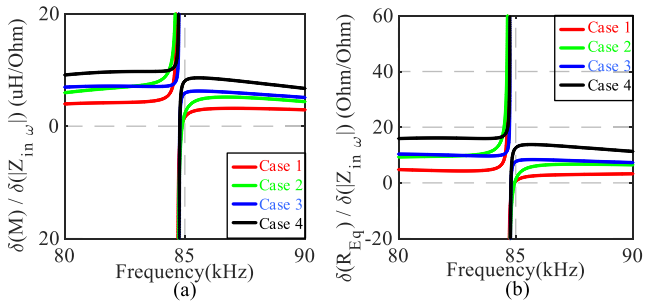

Fig. 17. Influence analysis of input impedance on (a) M, (b) R_{Eq}.

mean the collected data at the resonant point is poor. If the sensor circuit has very small noise, this point is still be usable. Besides, the resonant point has already been adopted for parameter identification, for instance, in [20], the fundamental harmonic and the third harmonic are used for identification.

F. Influence of C_1 and C_2

In experiment above, the actual values of C_1 and C_2 are the same as nominal values. But in actual applications, the values of C_1 and C_2 may deviate from the nominal values. Thus, the influence of capacitor deviation on M and R_{Eq} estimations should be analyzed. Following is the analyzing process: first, mathematical functions are analyzed; then, estimations under deviations of C_1 and C_2 are conducted; finally, the conventional method to solve the capacitor influence is applied and possible solutions to further improve the accuracy are introduced.

First, based on (10), by taking the derivative of $M\,(R_{Eq})$ to C_1 and C_2, the rate of change of $M\,(R_{Eq})$ with respect to C_1 and C_2 can be represented as (11) and (12), where $\delta M/\delta C_1$ and $\delta M/\delta C_2$ represent the partial derivative of M to C_1 and C_2 respectively; $\delta R_{Eq}/\delta C_1$ and $\delta R_{Eq}/\delta C_2$ represent the partial derivative of R_{Eq} to C_1 and C_2 respectively

$$\begin{cases} \frac{\delta M}{\delta C_1} = \frac{\sqrt{-\frac{E(A+C_1^2\omega^2 B-C+1)}{C_1 C_2 D}}(A-C_1^2\omega^2 B-C+1)}{2C_1\omega^2 D(A+C_1^2\omega^2 B-C+1)} \\ \frac{\delta M}{\delta C_2} = \frac{\sqrt{-\frac{E(A+C_1^2\omega^2 B-C+1)}{C_1 C_2 D}}}{2C_1\omega^2 E} \\ A = C_1^2\omega^3 L_1(\omega L_1 - 2|Z_{in\_\omega}|\sin\varphi) \\ B = R_1^2 - 2R_1|Z_{in\_\omega}|\cos\varphi \\ +(|Z_{in\_\omega}|\sin\varphi)^2 + (|Z_{in\_\omega}|\cos\varphi)^2 \\ C = 2C_1\omega(\omega L_1 - |Z_{in\_\omega}|\sin\varphi) \\ D = C_1\omega|Z_{in\_\omega}|\sin\varphi - C_1\omega^2 L_1 + 1 \\ E = C_2\omega^2 L_2 - 1 \end{cases} \tag{11}$$

$$\begin{cases} \frac{\delta R_{Eq}}{\delta C_1} = -\frac{(R_1 - |Z_{in\_\omega}|\cos\varphi)(C_2\omega^2 L_2 - 1)}{C_2(C_1\omega|Z_{in\_\omega}|\sin\varphi - C_1 L_1 + 1)^2} \\ \frac{\delta R_{Eq}}{\delta C_2} = \frac{C_1(R_1 - |Z_{in\_\omega}|\cos\varphi)}{C_2^2(C_1\omega|Z_{in\_\omega}|\sin\varphi - C_1 L_1 + 1)} \end{cases}. \tag{12}$$

With (11) and (12), the sensitivities can be derived as Fig. 18, where the partial derivative of C_1 (C_2) is in the second and fourth (first and third) quadrants. According to Fig. 18, the absolute values in the second and fourth quadrants are larger than that in

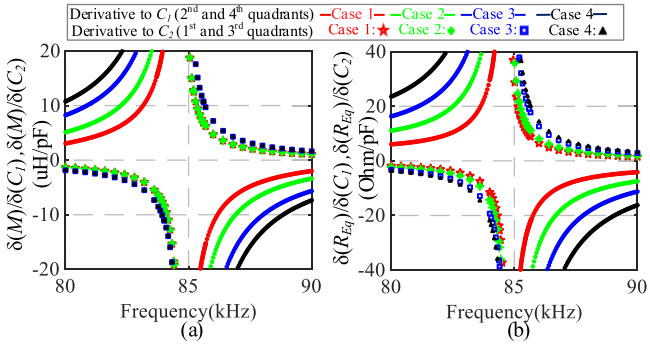

Fig. 18. Influence analysis of C_1 and C_2 on (a) M, (b) R_{Eq}.

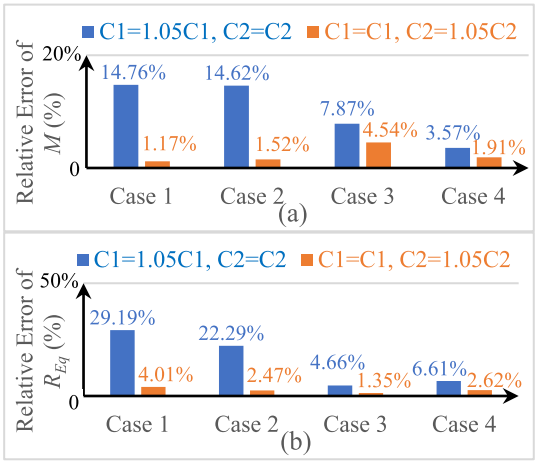

Fig. 19. Estimations under 5% deviation of C_1 and C_2 (a) M estimation, (b) R_{Eq} estimation.

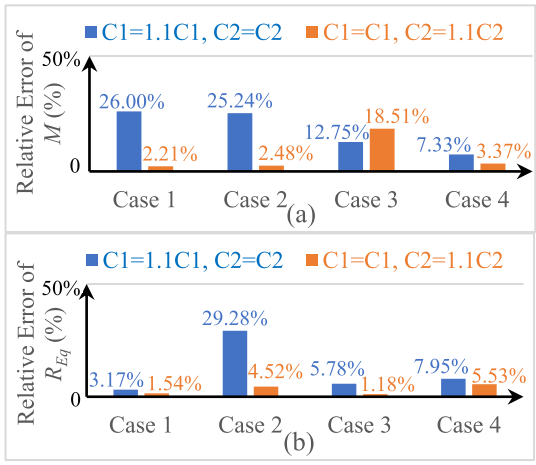

Fig. 20. Estimations under 10% deviation of C_1 and C_2 (a) M estimation, (b) R_{Eq} estimation.

TABLE VII
ESTIMATIONS FOR THE FOUR UNKNOWNS

	M (uH), Relative Error	R_{Eq} (Ω), Relative Error	C_1 (nF), Relative Error	C_2 (nF), Relative Error
Case 1	13.75, 5.17%	9.28, 4.63%	40.04, 2.20%	55, 8.67%
Case 2	14.07, 3%	12.04, 0.99%	40.04, 2.20%	55, 8.67%
Case 3	20.11, 1.76%	16.51, 7.40%	40.06, 0.77%	45.24, 9.32%
Case 4	19.63, 4.10%	18.52, 3.87%	39.93, 1.09%	42.87, 14.07%

TABLE VIII
PARAMETERS FOR LEAST-SQUARE APPROXIMATION

Parameter	M	R_{Eq}	C_1	C_2
[lower bound, upper bound]	[5uH, 30uH]	[1Ω, 30Ω]	[35nF, 45nF]	[45nF, 55nF]

the first and third quadrants, which means that the estimations are likely to be more sensitive to the variation of C_1 than that of C_2.

Then, with the data collected from the experiment in Fig. 12, the estimation results at the 14th point under 5% and 10% capacitor deviation are shown in Figs. 19 and 20, respectively. In these two pictures, blue bars represent the condition that C_1 deviates from the nominal value and C_2 is the nominal value, while the orange bars represent the condition that C_2 deviates from the nominal value and C_1 is the nominal value. Based on Fig. 19 (see Fig. 20), with 5% (10%) deviation of the capacitor, the maximum relative error for the orange bars is within 5% (19%), while for the blue bars reaches 30% (30%). Thus, the impact of C_1 is larger than that of C_2, this conclusion is in accordance with the mathematical analysis in Fig. 18.

Finally, it is mentioned in [17] and [18] that the capacitors should be considered as unknowns for estimation to solve the problem of capacitance deviation. Based on the data collected from the experiment in Fig. 12, the estimation results at the 14th point for these four unknowns are concluded as Table VII, where the parameters used in the least-square approximation are shown in Table VIII. In Figs. 19 and 20, the maximum relative errors for M and R_{Eq} reach 30%, and the error is proportional to the deviation of the capacitor, while in Table VII, the maximum relative errors for M and R_{Eq} are 5.17% and 7.40%. Therefore, under capacitance deviation, regarding capacitors as unknowns can obtain a much more accurate estimation than that of directly using the nominal capacitors values.

The comparisons of this estimation and other papers are concluded in Table IX, which is sorted from large relative error to small relative error. It can be concluded that the estimation accuracy of this experiment is an average level. These components play an important role in affecting the estimation accuracy: first, Algorithm of estimation. Among the algorithms in Table IX, equation calculation is the fastest and most accurate way for estimation, but it is only suitable for identifying one or two unknowns. Least-square approximation is relatively less accurate because it involves approximate equations to simplify the functions. second, hardware circuits of data obtaining. The results in [36] demonstrate that the error of sampling circuits contributes much to the estimation error, and optimizing the sampling circuits will improve the accuracy. Since the algorithm and hardware are not the focus of this article, they will not be further discussed.

TABLE IX
COMPARISON OF THE PARAMETER IDENTIFICATION METHODS

	Estimated Parameter	Estimation Algorithm (Estimation Speed)	Maximum Relative Error for M, R_{eq}
[37]	M, R_{Eq}	Equation calculation (Fast)	8% for M, 12.9% for R_{eq}
[13]	R_{Eq}	4th-order differential approximation (Fast)	> 7%
Proposal with capacitor deviation	M, R_{Eq}, C_1, C_2	Least-square approximation (Relative fast)	5.17% for M, 7.40% for R_{eq}
[38]	M, R_{Eq}	Equation calculation (Fast)	6.68% for M, 5.60% for R_{eq}
[19]		Ferrari Method (Fast)	5.70% for M, 5.50% for R_{eq}
[18]	M, R_{Eq}, C_2, L_2	Adaptive differential evolution (Slow)	< 5%
Proposal without capacitor deviation	M, R_{Eq}	Least-square approximation (Relative fast)	
[21]	R_{Eq}		

IV. CONCLUSION AND FUTURE WORK

In this article, a PDM-technology-based identification method for mutual inductance and load resistance is proposed. Although the interharmonics in PDM tech are previously considered as useless noises, this article presents an idea to use them for identifying parameters. The advantages of this proposal include no extra hardware, ZVS can be maintained, and the power and efficiency are not affected during the estimation process. Only information of voltage and current magnitudes on front-end is needed, and this method is applicable to other working frequencies and topologies. The limitation is that it requires 2–5 s for calculation, making it more suitable for stationary charging.

Capacitance deviation is possible in a real application, so, except estimations without capacitance deviation, the experiment also carries out the estimations with capacitance deviation. The results demonstrate that the relative errors of this experiment are at an average level compared with other identification methods.

This article selects sequence to maximize interharmonics, but in the normal charging process, smaller interharmoncs are preferred for less loss. So, the sequence investigation may be further studied for improving charging efficiency with PDM.

REFERENCES

[1] G. A. Covic and J. T. Boys, "Inductive power transfer," *Proc. IEEE*, vol. 101, no. 6, pp. 1276–1289, Jun. 2013.

[2] S. Q. Li and C. C. Mi, "Wireless power transfer for electric vehicle applications," *IEEE J. Emerg. Sel. Topics Power Electron.*, vol. 3, no. 1, pp. 4–17, Mar. 2015.

[3] H. H. Wu, A. Gilchrist, K. D. Sealy, and D. Bronson, "A high efficiency 5 kW inductive charger for EVs using dual side control," *IEEE Trans. Ind. Informat.*, vol. 8, no. 3, pp. 585–595, Aug. 2012.

[4] N. Liu and T. G. Habetler, "Design of a universal inductive charger for multiple electric vehicle models," *IEEE Trans. Power Electron.*, vol. 30, no. 11, pp. 6378–6390, Nov. 2015.

[5] Y. Xu *et al.*, "A switchable-LCL-circuit-based IPT system with high efficiency for reefer containers," *IEEE Trans. Power Electron.*, vol. 36, no. 2, pp. 1253–1258, Feb. 2021.

[6] W. Cai, H. Tang, X. Lai, and L. Sun, "Multiple-receiver wireless power transfer with efficient power control strategy," in *Proc. IEEE PELS Workshop Emerg. Technol., Wireless Power Transfer*, 2019, pp. 378–382.

[7] R. Mai, Y. Liu, Y. Li, P. Yue, G. Cao, and Z. He, "An active-rectifier-based maximum efficiency tracking method using an additional measurement coil for wireless power transfer," *IEEE Trans. Power Electron.*, vol. 33, no. 1, pp. 716–728, Jan. 2018.

[8] Z. Huang, S. Wong, and C. K. Tse, "Control design for optimizing efficiency in inductive power transfer systems," *IEEE Trans. Power Electron.*, vol. 33, no. 5, pp. 4523–4534, May 2018.

[9] S. Li and S. Y. R. Hui, "Comparative study on front-end parameter identification methods for wireless power transfer without wireless communication systems," in *Proc. Int. Power Electron. Conf.*, 2018, pp. 2552–2557.

[10] U. K. Madawala and D. J. Thrimawithana, "New technique for inductive power transfer using a single controller," *Power Electron. IET*, vol. 5, no. 2, pp. 248–256, 2012.

[11] U. K. Madawala and D. J. Thrimawithana, "A single controller for inductive power transfer systems," in *Proc. 35th Annu. Conf. IEEE Ind. Electron.*, 2009, pp. 109–113.

[12] Z. Wang, Y. Li, Y. Sun, C. Tang, and X. Lv, "Load detection model of voltage-fed inductive power transfer system," *IEEE Trans. Power Electron.*, vol. 28, no. 11, pp. 5233–5243, Nov. 2013.

[13] S. Hu, Z. Liang, Y. Wang, J. Zhou, and X. He, "Principle and application of the contactless load detection based on the amplitude decay rate in a transient process," *IEEE Trans. Power Electron.*, vol. 32, no. 11, pp. 8936–8944, Nov. 2017.

[14] Y. Su, H. Zhang, Z. Wang, A. Patrick Hu, L. Chen, and Y. Sun, "Steady-state load identification method of inductive power transfer system based on switching capacitors," *IEEE Trans. Power Electron.*, vol. 30, no. 11, pp. 6349–6355, Nov. 2015.

[15] Y. Yang, S. C. Tan, and S. Y. R. Hui, "Fast hardware approach to determining mutual coupling of series–series-compensated wireless power transfer systems with active rectifiers," *IEEE Trans. Power Electron.*, vol. 35, no. 10, pp. 11026–11038, Oct. 2020.

[16] J. Yin, D. Lin, T. Parisini, and S. Y. Hui, "Front-end monitoring of the mutual inductance and load resistance in a series–series compensated wireless power transfer system," *IEEE Trans. Power Electron.*, vol. 31, no. 10, pp. 7339–7352, Oct. 2016.

[17] D. Lin, J. Yin, and S. Y. R. Hui, "Parameter identification of wireless power transfer systems using input voltage and current," in *Proc. IEEE Energy Convers. Congr. Expo.*, 2014, pp. 832–836.

[18] Y. Yang, S. Tan, and S. Y. R. Hui, "Front-end parameter monitoring method based on two-layer adaptive differential evolution for SS-compensated wireless power transfer systems," *IEEE Trans. Ind. Informat.*, vol. 15, no. 11, pp. 6101–6113, Nov. 2019.

[19] X. Sheng and L. Shi, "Mutual inductance and load identification method for inductively coupled power transfer system based on auxiliary inverter," *IEEE Trans. Veh. Technol.*, vol. 69, no. 2, pp. 1533–1541, Feb. 2020.

[20] J. W. Liu, G. B. Wang, G. Xu, J. Peng, and H. Jiang, "A parameter identification approach with primary-side measurement for DC-DC wireless-power-transfer converters with different resonant tank topologies," *IEEE Trans. Transp. Electrific.*, vol. 7, no. 3, pp. 1219–1235, Sep. 2021.

[21] J. Yin, D. Y. Lin, C. K. Lee, T. Parisini, and S. Y. Hui, "Front-end monitoring of multiple loads in wireless power transfer systems without wireless communication systems," *IEEE Trans. Power Electron.*, vol. 31, no. 3, pp. 2510–2517, Mar. 2016.

[22] G. B. Joung, C. T. Rim, and G. H. Cho, "An integral cycle mode control of series resonant converter," in *Proc. 19th Annu. IEEE Power Electron. Specialists Conf.*, Apr. 1988, pp. 575–582, vol. 2.

[23] H. Fujita and H. Akagi, "Pulse-density-modulated power control of a 4 kW, 450 kHz voltage-source inverter for induction melting applications," *IEEE Trans. Ind. Appl.*, vol. 32, no. 2, pp. 279–286, Mar./Apr. 1996.

[24] H. Calleja and J. Pacheco, "Power distribution in pulse-density modulated waveforms," in *Proc. IEEE 31st Annu. Power Electron. Specialists Conf.. Conf. Proc.*, Jun. 2000, pp. 1457–1462, vol. 3.

[25] A. Testa *et al.*, "Interharmonics: Theory and modeling," *IEEE Trans. Power Del.*, vol. 22, no. 4, pp. 2335–2348, Oct. 2007.

[26] H. C. Li, K. Wang, J. Fang, and Y. Tang, "Pulse density modulated ZVS full-bridge converters for wireless power transfer systems," *IEEE Trans. Power Electron.*, vol. 34, no. 1, pp. 369–377, Jan. 2019.

[27] Y. Chen *et al.*, "Reconfigurable topology for IPT system maintaining stable transmission power over large coupling variation," *IEEE Trans. Power Electron.*, vol. 35, no. 5, pp. 4915–4924, May 2020.

[28] Q. Duong and M. Okada, "Maximum efficiency formulation for multiple-input multiple-output inductive power transfer systems," *IEEE Trans. Microw. Theory Techn.*, vol. 66, no. 7, pp. 3463–3477, Jul. 2018.
[29] S. J. W. Jorge Nocedal, "Numerical optimization," in *Outline of the Trust-Region Approach*, New York, NY, USA: Springer, 2006, pp. 66–70, Ch. 4.
[30] C. Ouyang, S. Wu, C. Jiang, J. Cheng, A. Xiao, and H. Yang, "Security enhancement via antenna selection in MIMOME channels with discrete inputs," *IEEE Trans. Commun.*, vol. 68, no. 8, pp. 5041–5055, Aug. 2020.
[31] M. Y. Fan, L. M. Shi, Z. G. Yin, L. Jiang, and F. Zhang, "Improved pulse density modulation for semi-bridgeless active rectifier in inductive power transfer system," *IEEE Trans. Power Electron.*, vol. 34, no. 6, pp. 5893–5902, Jun. 2019.
[32] F. Zhou, "Online estimation algorithm for harmonic and interharmonic in power systems based on the quasi-synchronous sampling,", Ph.D. dissertation, Dept. School Electron. Inf. Elect. Eng., Shanghai Jiao Tong Univ., Shanghai, China, 2012.
[33] X. R. Sheng and L. Shi, "An improved pulse density modulation strategy based on harmonics for ICPT system," *IEEE Trans. Power Electron.*, vol. 35, no. 7, pp. 6810–6819, Jul. 2020.
[34] M. K. Kazimierczuk and D. Czarkowski, "Class d series-resonant inverters," in *Resonant Power Converters*, 2nd ed. Hoboken, NJ, USA: Wiley, 2011, Art. no. 184, Ch. 6.
[35] M. K. Kazimierczuk and D. Czarkowski, "Class D current-driven rectifiers," in *Resonant Power Converters*, 2nd ed. Hoboken, NJ, USA: Wiley, 2011, P.31, Ch. 2.
[36] S. Li, L. Wang, Y. Guo, and Z. Liu, "Flexible energy-transfer control of dynamic wireless power transfer system based on estimation of load and mutual inductance," *IEEE Trans. Ind. Appl.*, vol. 58, no. 1, pp. 1157–1167, Jan./Feb. 2022.
[37] X. Dai, Y. Sun, and C. Tang, "Dynamic parameters identification method for inductively coupled power transfer system," in *Proc. IEEE Int. Conf. Sustain. Energy Technol.*, 2011, pp. 1–5.
[38] Y. Su *et al.*, "Load and mutual inductance identification from the primary side of inductive power transfer system with parallel-tuned secondary power pickup," *IEEE Trans. Power Electron.*, vol. 33, no. 11, pp. 9952–9962, Nov. 2018.

Ruimin Dai received the B.E. degree from Southwest Jiaotong University, Chengdu, China, in 2014, and the M.S. degree from Stony Brook University, Stony Brook, NY, USA, in 2015. She is currently working toward the Ph.D. degree from Southwest Jiaotong University.

Her current research interests include wireless power transfer.

Wei Zhou (Member, IEEE) received the B.E. and Ph.D. degrees from the School of Automation, Chongqing University, Chongqing, China, in 2013 and 2018, respectively.

He was with the Department of Electrical, Computer and Software Engineering, The University of Auckland, Auckland, New Zealand, from 2016 to 2017, as a Visiting Scholar. He is currently a Lecturer with the School of Electrical Engineering, Southwest Jiaotong University, Chengdu, China. His current research interests include wireless power transfer technologies.

Yonghong Chen received the B.S. degree in petroleum engineering from Southwest Petroleum University, Chengdu, China, in 2018. He is currently working toward the M.E.E degree with the School of Electrical Engineering, Southwest Jiaotong University, Chengdu, China.

His research interest focuses on wireless power transfer.

Zhehui Zhu was born in Hunan, China, in 1997. He received the B.Sc. degree from the Changsha University of Science and Technology, Changsha, China, in 2018, and the M.Sc. degree from Southwest Jiaotong University, Chengdu, China, in 2021.

He is currently an Electrical Engineer with National Engineering Research Center of Converters, Zhuzhou, China. His current research interest focuses on wireless power transfer.

Ruikun Mai received the B.Sc. and Ph.D. degrees in electrical engineering from the School of Electrical Engineering, Southwest Jiaotong University, Chengdu, China, in 2004 and 2010, respectively.

He is currently a Professor with the School of Electrical Engineering, Southwest Jiaotong University, Chengdu, China. His research interests include wireless power transfer and its application in railway systems, power system stability, and control.